Research in Education, Technology, and Multiculture
ISSN: 3025-6763 | Journal's DOI: 10.61436/rietm
Homepage: https://imrecsjournal.com/journals/index.php/rietm

Effects of Indoor Unit Height and Airflow Distribution on Cooling Performance and Energy Consumption in Inverter and Non-Inverter Air Conditioners

Agustinus Djoko Istiadji*, & Frengky Benediktus Ola
Department of Architecture, Universitas Atma Jaya, Indonesia

ARTICLE INFO
Article History:
Received: 10 August 2026
Accepted: 03 September 2026
Published: 12 September 2026

Keywords:
Airflow distribution;
Air conditioning technology;
Energy efficiency;
Indoor unit installation.

Corresponding Author:
ag.istiadji@gmail.com

ABSTRACT
Residential buildings are the largest contributors to electricity consumption, with air conditioning (AC) systems being one of the primary consumers of electricity. Energy-saving strategies involving physical modifications to buildings are often difficult to implement in existing structures because they require high costs and large-scale structural changes. Therefore, optimizing air conditioning performance by regulating indoor airflow distribution offers a more practical alternative for improving energy efficiency. This study aims to analyze the effect of airflow distribution patterns, resulting from variations in indoor-unit installation height, on cooling performance and energy consumption in inverter and non-inverter split AC systems through laboratory experiments in a controlled test chamber. Three air distribution configurations were tested: Perfect Mixing Above (PM_Above), Perfect Mixing Middle (PM_Middle), and Displacement (D_Bottom), each combined with two occupant layouts: facing the air conditioner directly and positioned along the wall edge. The observed parameters included the rate of temperature drop, the time required to reach a comfortable temperature, indoor temperature distribution, and electricity consumption. The results showed that air conditioning performance is influenced by the interaction between compressor technology and airflow distribution patterns, rather than solely by cooling capacity. The PM_Middle configuration achieves the best balance between cooling effectiveness and energy efficiency for both inverter and non-inverter air conditioners, and inverter air conditioners with this configuration proved the most suitable choice for long-term use in residential buildings.

To cite this article:
Istiadji, A. D., & Ola, F. B. (2026). Effects of indoor unit height and airflow distribution on cooling performance and energy consumption in inverter and non-inverter air conditioners. *Research in Education, Technology, and Multiculture*, *5*(3), 329-348. doi: https://doi.org/10.61436/rietm/v5i3.pp329-348

INTRODUCTION

Fossil fuels still dominate Indonesia's national energy supply, accounting for around 81% of the total energy supply (Kementerian ESDM, 2025; Setyawati & Setiawan, 2024; Yudiartono et al., 2023). This high dependence on these energy sources has not been matched by a commensurate increase in supply capacity, potentially increasing the risk of a future energy crisis. This situation makes improving energy efficiency an increasingly important strategy.

The residential sector is the largest contributor to national electricity consumption and has the highest energy consumption rate of all sectors (Ali et al., 2024; Cahyani et al., 2022). Data from PT PLN (Persero) show that electricity consumption in the residential sector reached 67.14 TWh in the first half of 2025, an increase of 5.13 percent from the same period the previous year, as a proportion of total national electricity sales (PLN, 2025). This indicates that improving energy efficiency in the residential sector could significantly reduce national electricity consumption.

Air conditioning (AC) systems are one of the main contributors to electricity consumption in the residential sector. Previous studies have reported that electricity consumption in homes fitted with air conditioning is around 36% higher than in homes without air conditioning (De Cian et al., 2025; Liddle et al., 2020). These findings suggest that improving the operational efficiency of air conditioners could contribute to energy-saving efforts in the residential sector. This urgency is strengthened by data on air conditioner sales in Indonesia, which shows the dominance of non-inverter split-type units, particularly those with a capacity of 0.5 HP and a three-star energy efficiency rating.

There are generally three approaches to improving the energy efficiency of air conditioning systems: optimizing the passive design of the building envelope, implementing more efficient air conditioning technology, and adjusting airflow distribution within the room. The first option is difficult to implement in existing buildings, as it usually requires structural modifications and involves high costs (Citadini de Oliveira et al., 2024; Welch et al., 2023). The second strategy involves switching to energy-efficient technologies, such as inverter technology. Inverter technology in air conditioners can reduce energy consumption by 35-44 percent compared with non-inverter air conditioners (Almogbel et al., 2020). The third strategy, optimizing airflow distribution, is also relatively easier to implement in existing buildings as it does not require alterations to the building's structure itself; however, its impact on cooling performance and energy efficiency is not yet fully understood, particularly in residential settings (Kar & Abedin, 2025; Wang et al., 2023). Previous studies have documented the importance of airflow distribution in determining cooling system performance, showing that airflow patterns directly affect occupants' thermal comfort and the overall performance of the air-conditioning system (Wang et al., 2023).

Nevertheless, air-conditioning installation in residential buildings in Indonesia generally still adopts a 'perfect mixing' configuration, with units mounted at the top of the wall. This configuration can result in inconsistent temperature distribution within the space (Barau et al., 2024). In practice, air-conditioning unit positioning is often based on installation convenience and available wall space, while the impact of installation height, airflow direction, and airflow distribution patterns on system performance is rarely considered (Jin et al., 2022; Kwag et al., 2023). Consequently, the potential to improve energy efficiency by optimizing airflow distribution has not yet been fully utilized.

Inverter technology, on the other hand, has become an effective approach to improving energy efficiency in air-conditioning systems. Inverter air conditioners with operating modes adapted to the climate can even decrease energy consumption by up to 45% (Almogbel et al., 2020). Although this technology offers considerable energy-saving potential, its adoption rate in Indonesia remains relatively low. Research estimates that only around 5 percent of the 3.97 million domestic air-conditioning units currently use inverter technology (De Cian et al., 2025). This indicates that most households still rely on non-inverter air conditioners; therefore, improving energy efficiency requires not only developing more energy-efficient technologies but also optimizing the performance of units already in widespread use.

In this context, this study aims to compare the performance of inverter-type and non-inverter-type air conditioners in achieving the target room temperature and to evaluate how airflow distribution patterns affect cooling effectiveness and energy consumption. Unlike previous studies, which generally focused on either technological efficiency or air distribution separately, this study examines the interaction between these two factors in wall-mounted split-type air-conditioning systems commonly used in residential buildings in Indonesia. Therefore, this study aims to recommend air-conditioning installation configurations that improve both cooling effectiveness and energy efficiency. Based on this background, this study aims to answer three research questions, as follows: (1) How do installation height and airflow distribution patterns affect the cooling rate and the time required to reach the target temperature in the occupied zone, for both inverter and non-inverter air conditioners? (2) How does the interaction between compressor technology (inverter and non-inverter) and airflow distribution patterns affect energy consumption across various test configurations? (3) What combination of installation height and fan speed is capable of providing the most optimal balance between cooling effectiveness, energy efficiency, and occupants' thermal comfort?

■ METHOD

This study employed a quantitative method using laboratory experiments to evaluate the effect of airflow distribution on cooling performance and energy consumption in wall-mounted split-type air-conditioning systems. All experiments were conducted in a climate-controlled laboratory to keep environmental conditions under control. Controlled laboratory testing can minimize the influence of external factors that could cause variations in results and lead to data inconsistencies (Aziz, 2017). This study examined two main variables: air-conditioning technology (inverter and non-inverter) and airflow distribution patterns. The latter were created by varying the indoor unit installation height and fan speed. These two variables produced 24 test scenarios, each evaluated independently to identify the configuration that best balanced cooling effectiveness and energy efficiency.

To improve clarity, this section divides the research methodology into four subsections that describe the main stages and components of the research. These subsections include (1) the experimental design and test facilities, which describe the air-cooled test chamber; (2) the specifications of the equipment and instruments used; (3) the research variables and test configurations, covering the independent, dependent, and controlled variables; and (4) the test procedures and data collection.

The Experimental Design

Air cooling test chamber

The testing was carried out in a test chamber measuring 13.8 m² and 3 m high, as shown in Figure 1. These dimensions were chosen because they match the size of rooms typically found in residential homes and align with previous research (Pisello et al., 2021; Sekhar et al., 2021). This previous research used test chambers measuring approximately 9-15 m² to evaluate the performance of air conditioning systems. The chamber walls were constructed with materials having a U-value of 3,26 W/m2K, and the ambient temperature in the surrounding space was maintained at 31-30°C to control for heat penetration rates and ensure experimental replicability. Therefore, the room layout is assumed to accurately reflect how air-conditioning units operate in homes. This test facility comprises three areas: the experimental room, the preparation room, and the climate chamber. Participants undergo thermal acclimatization in these rooms before testing.

Therefore, the room layout is assumed to accurately reflect how air-conditioning units operate in homes. This test facility comprises three areas: the experimental room, the preparation room, and the climate chamber. Participants undergo thermal acclimatization in these rooms before testing.

In this study, two wall-mounted split-type air conditioning units were used: one inverter and one non-inverter unit, each with a rated capacity of 8,500 BTU or more. The inverter unit had a nominal Energy Efficiency Ratio (EER) of approximately 12.50 Btu/Wh, a Cooling Seasonal Performance Factor (CSPF) of 6.35 W/W, and a maximum airflow of 332 CFM (564 CMH). The non-inverter unit featured a nominal EER of approximately 11.92 Btu/Wh, a CSPF of 3.59 W/W, and a maximum airflow of 360 CFM (612 CMH). Both units used R-32 refrigerant, and selecting units with similar cooling capacity minimized this factor, allowing for a more accurate evaluation of the primary variables.

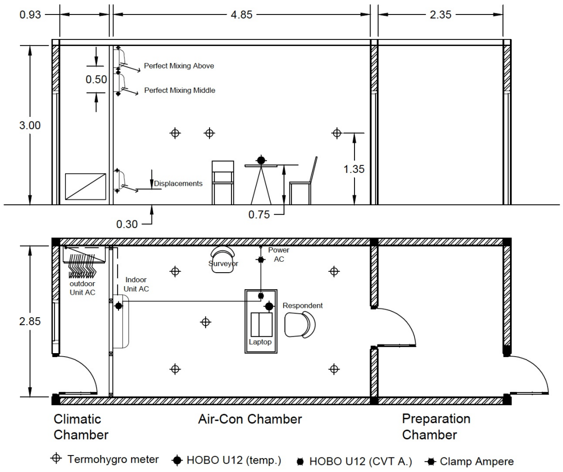

Figure 1. Measurement room plans

Specifications of The Equipment and Instruments Used

This study used four types of instruments to measure environmental parameters and energy consumption during testing, as shown in Figure 2. These instruments were selected according to the parameters being measured, as follows: (1) Thermohygrometers (5 units): placed at specified measurement points to measure air temperature and humidity at various vertical heights within the test chamber. (2) HOBO U12 Data Loggers (3 units): placed on the air conditioning unit and on the respondent's desk; these devices automatically recorded temperature changes every two minutes, enabling continuous documentation of temperature profiles throughout the testing. (3) Clamp ampere meter (1 unit): used to manually measure electrical current by clamping onto the power supply cable of the air conditioning unit during each testing session. (4) Continuous wattmeter (1 set): used to record electricity consumption in real time throughout the test period, thereby enabling the continuous collection of energy usage data.

Figure 2. The instruments used in data collection

Variables and Testing Configurations

In this study, variables were categorized as independent, dependent, and controlled. The independent variables included air-conditioning technology, indoor-unit installation height, fan speed, and workspace layout. The air-conditioning technologies tested comprised two types: inverter and non-inverter air conditioners. The indoor units were tested at three installation heights representing different airflow distribution patterns: Perfect Mixing Above (PM_A), Perfect Mixing Middle (PM_M), and Displacement (D_Bottom). In the PM_Above configuration, the indoor unit was installed 2.6 m above the floor, representing the standard installation height for split air-conditioning units in residential buildings. In the PM_Middle configuration, the unit was installed at 2.1 m above the floor to examine the effect of a lower installation height on airflow characteristics and cooling performance. In the Displacement configuration, the unit was installed 0.3 m above the floor to represent a bottom-up airflow distribution pattern. Each installation-height variation was then combined with two fan speed levels: F2 (1.5 m/s) and F4 (1.7 m/s). These fan-speed variations were used to evaluate the effect of airflow velocity on cooling performance. In this study, two workspace layout configurations were applied to examine the effect of workspace position on airflow distribution and thermal conditions within the room. In Configuration MD, the workspace faced the air-conditioning unit, while in Configuration SD, the workspace was positioned at the side of the room.

The dependent variables in this study were used to evaluate the cooling performance, energy efficiency, and thermal conditions produced by each experimental configuration. These variables included the rate of temperature decrease, the time required to reach the target temperature, the spatial distribution of temperature within the occupied zone, and electricity consumption. The rate of temperature decrease characterized the room’s cooling response. In contrast, the time required to reach the target temperature was used to assess each configuration's effectiveness in achieving the target thermal conditions. The spatial distribution of temperature was used to identify variations in thermal conditions within the occupied zone. In contrast, the electricity consumption was used to evaluate the energy performance of each cooling configuration.

To ensure that differences across scenarios were primarily due to changes in the independent variables, several conditions were held constant. First, the initial room temperature was set at 29°C before each test, while the target temperature was set at 25°C for all scenarios. Second, the air conditioning units used had the same nominal cooling capacity: 8,500 BTU. Furthermore, the test chamber dimensions and physical characteristics, as well as the test procedures, were kept consistent across all scenarios.

The combination of two types of air-cooling technology, three indoor-unit installation heights, two fan speed levels, and two workspace layout configurations resulted in 24 test scenarios (2 × 3 × 2 × 2). Each scenario was tested independently four times, with one participant per test session. These repetitions were carried out to enhance the

Table 1. Matrix of the 24 test scenarios

No	AC Technology	Installation Height	Fan Speed	Workspace Layout	Experiment Code
1	Non-Inverter	PM_Above (2.6 m)	F2 (1.5 m/s)	MD (facing the air-conditioning unit)	NI_PMA_F2_MD
2	Non-Inverter	PM_Above (2.6 m)	F2 (1.5 m/s)	SD (side of the room)	NI_PMA_F2_SD
3	Non-Inverter	PM_Above (2.6 m)	F4 (1.7 m/s)	MD (facing the air-conditioning unit)	NI_PMA_F4_MD
4	Non-Inverter	PM_Above (2.6 m)	F4 (1.7 m/s)	SD (side of the room)	NI_PMA_F4_SD
5	Non-Inverter	PM_Middle (2.1 m)	F2 (1.5 m/s)	MD (facing the air-conditioning unit)	NI_PMM_F2_MD
6	Non-Inverter	PM_Middle (2.1 m)	F2 (1.5 m/s)	SD (side of the room)	NI_PMM_F2_SD
7	Non-Inverter	PM_Middle (2.1 m)	F4 (1.7 m/s)	MD (facing the air-conditioning unit)	NI_PMM_F4_MD
8	Non-Inverter	PM_Middle (2.1 m)	F4 (1.7 m/s)	SD (side of the room)	NI_PMM_F4_SD

9	Non-Inverter	Displacement (0.3 m)	F2 (1.5 m/s)	MD (facing the air-conditioning unit)	NI_D_BOTTOM_F2_MD
10	Non-Inverter	Displacement (0.3 m)	F2 (1.5 m/s)	SD (side of the room)	NI_D_BOTTOM_F2_SD
11	Non-Inverter	Displacement (0.3 m)	F4 (1.7 m/s)	MD (facing the air-conditioning unit)	NI_D_BOTTOM_F4_MD
12	Non-Inverter	Displacement (0.3 m)	F4 (1.7 m/s)	SD (side of the room)	NI_D_BOTTOM_F4_SD
13	Inverter	PM_Above (2.6 m)	F2 (1.5 m/s)	MD (facing the air-conditioning unit)	I_PMA_F2_MD
14	Inverter	PM_Above (2.6 m)	F2 (1.5 m/s)	SD (side of the room)	I_PMA_F2_SD
15	Inverter	PM_Above (2.6 m)	F4 (1.7 m/s)	MD (facing the air-conditioning unit)	I_PMA_F4_MD
16	Inverter	PM_Above (2.6 m)	F4 (1.7 m/s)	SD (side of the room)	I_PMA_F4_SD
17	Inverter	PM_Middle (2.1 m)	F2 (1.5 m/s)	MD (facing the air-conditioning unit)	I_PMM_F2_MD
18	Inverter	PM_Middle (2.1 m)	F2 (1.5 m/s)	SD (side of the room)	I_PMM_F2_SD
19	Inverter	PM_Middle (2.1 m)	F4 (1.7 m/s)	MD (facing the air-conditioning unit)	I_PMM_F4_MD
20	Inverter	PM_Middle (2.1 m)	F4 (1.7 m/s)	SD (side of the room)	I_PMM_F4_SD
21	Inverter	Displacement (0.3 m)	F2 (1.5 m/s)	MD (facing the air-conditioning unit)	I_D_BOTTOM_F2_MD
22	Inverter	Displacement (0.3 m)	F2 (1.5 m/s)	SD (side of the room)	I_D_BOTTOM_F2_SD
23	Inverter	Displacement (0.3 m)	F4 (1.7 m/s)	MD (facing the air-conditioning unit)	I_D_BOTTOM_F4_MD
24	Inverter	Displacement (0.3 m)	F4 (1.7 m/s)	SD (side of the room)	I_D_BOTTOM_F4_SD

reliability and reproducibility of the experimental results. To present the 24 test scenarios more clearly, the combinations are shown in Table 1.

Testing Procedure

All experimental scenarios used the same testing procedure to ensure consistent testing conditions across configurations. Each testing scenario involved one respondent and one researcher, who recorded data manually and supervised the experiment. The respondents in the study were students aged between 22 and 25; the thermal insulation of their clothing was estimated to be in the range of 0.58-0.63 clo, which is typical for thin indoor clothing, and their metabolic rates were consistent with sedentary activity (approximately 1.1 met), involving sitting and performing light computer work. The experiment was conducted in two stages: preparation and data collection. During the preparation phase, the door between the test chamber and the outside area was left open for approximately 60 minutes. During this period, the test chamber temperature was monitored while being allowed to rise gradually until it reached the initial temperature of 29°C. Fluctuations in the test chamber temperature during the preparation stage are presented in Figure 3. Data collection began after the test chamber temperature reached 29°C and remained stable for at least 5 minutes. The 5-minute stabilization period was set because this study aims to observe the transient cooling characteristics and energy consumption of the air conditioning unit during the first 60 minutes of operation, rather than determining how long it takes for the air conditioner to stabilize its energy consumption and cool the room. An initial temperature of 29°C was applied to all test scenarios to ensure each experiment started from the same thermal conditions, allowing

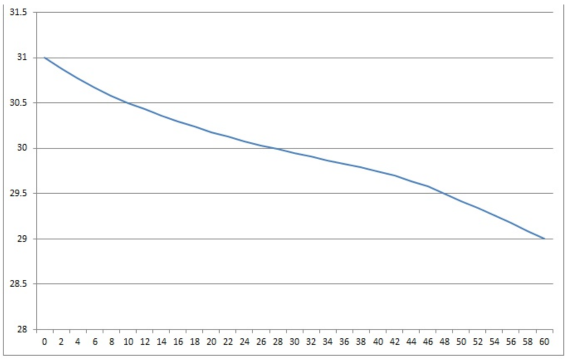

Figure 3. Temperature fluctuations in the test chamber

consistent comparison across scenarios. Controlling the initial thermal conditions is crucial because environmental conditions prior to testing can influence the system's thermal response and experimental results (Gnecco et al., 2025; Van Craenendonck et al., 2018; Zhai et al., 2019). However, these studies did not specify a standard duration for the preparation phase, as the time required to reach the initial conditions depends on each study's objectives and design.

The next stage was data collection, conducted over 60 minutes for each test scenario. During this period, air temperature and electricity consumption were recorded every two minutes, either automatically using a data logger or manually by the researchers. At the same time, participants completed a thermal comfort perception questionnaire every two minutes, as shown in Figure 3. These subjective assessments complemented the environmental measurements, as thermal comfort is a subjective response that cannot be fully determined from environmental parameters such as air temperature alone.

This study used the Bedford Scale, modified into five response categories: cold, cool, comfortable, warm, and hot. This modification simplified the response options and aligned them with the study's objective: to identify respondents' thermal conditions more directly and to separate comfort from conditions perceived as too cold or too hot. Previous studies have used a modified approach to the Bedford Scale (Cosma & Simha, 2018), including combining several categories from the original scale into simpler categories aligned with the study's comfort evaluation objectives.

During the test, respondents were not provided with information regarding the actual temperature inside the test chamber to minimize the possibility that knowledge of environmental conditions might influence their subjective assessments. Consequently, the responses provided were expected to represent their direct thermal perceptions. This subjective data was then used to supplement and validate the interpretation of thermal comfort levels based on objective measurement results.

Figure 4. The procedure of data collection

Research Limitations

This study has several limitations: data collection was carried out in a controlled test environment, meaning that the results do not account for other variables such as the simultaneous use of electrical appliances and changes in outdoor air infiltration. Because this study involved university students, its findings are expected to be most relevant to living spaces such as bedrooms or student accommodation.

Furthermore, this study evaluated only wall-mounted split-type air conditioners; therefore, the results cannot be directly generalized to other cooling systems without separate testing. The comparison between inverter and non-inverter air conditioners also used only one unit of each type with the same cooling capacity (8,500 BTU); differences in product characteristics may still contribute to the observed performance differences.

A factorial analysis of variance (ANOVA) was conducted to evaluate the effects of compressor technology, indoor-unit installation height, fan speed, and workstation layout on energy consumption and the time required to reach a comfortable temperature. However, this statistical analysis has several limitations. The assumptions of normality of residuals and homogeneity of variances were not fully met, as indicated by the Shapiro-Wilk and Levene's tests (https://www.semanticscholar.org/paper/An-Analysis-of-Variance-Test-for-Normality-Samples)-Shapiro-Wilk/e4a742a4f0585b4e4069726f6628f4d4285a0827). The ANOVA results were interpreted in conjunction with the descriptive findings and supported by non-parametric robustness tests.

For the analysis of the time taken to reach comfort, the 'Displacement' configuration was not included in the factorial ANOVA because none of the observations reached a comfortable temperature within the 60-minute observation period. The statistical analysis of the time taken to reach the target temperature was restricted to the 'PM_Above' and 'PM_Middle' configurations. These limitations should be considered when interpreting statistical differences between the installation-height configurations.

■ RESULT AND DISCUSSION

Setting a Comfortable Temperature

To evaluate how quickly non-inverter and inverter air conditioners cool in all configurations, this study first established a comfort temperature as a baseline. This comfort temperature was determined based on respondents' perceptions of comfort and then validated using applicable room-temperature comfort standards and a review of relevant literature.

The measurement results showed that respondents felt comfortable at an ambient room temperature of 24.43°C and an occupancy point temperature of 25.77°C. These values were then compared with several currently applicable thermal comfort standards. SNI 03-6572-2001 specifies an effective temperature range of 20.5-27.1°C, with the "cool and comfortable" category at 20.2-22.8°C, "optimal" at 22.8-25.8°C, and "warm but not too hot" at 25.8-47.2°C (Badan Standarisasi Nasional, 2001). Meanwhile, ASHRAE 55 recommends a range of 23-26°C for light activities while wearing insulating clothing (ASHRAE, 2004), and Ministry of Health Regulation No. 48 of 2016 on Occupational Safety and Health Standards for Offices sets the office room temperature range at 23-26°C to meet health and comfort requirements (Kementerian Kesehatan, 2016).

In addition to being validated by standards, these findings are also supported by several literature reviews on comfortable temperature conditions. A study on comfortable workplace temperatures in Japan found that 70% of respondents felt comfortable at a room temperature of 25°C (Maharjan & Rijal, 2026). Another study in Brazil reported that 80% of classroom users felt comfortable within a temperature range of 23-24°C (Buonocore et al., 2020). Furthermore, differences in thermal comfort perception of less than 5% are common, as these perceptions are influenced by subjective individual characteristics (Khorram et al., 2020). In contrast, in this study, the difference was less than 2%. Therefore, based on the respondents' questionnaire results and a comparison with the thermal comfort standards mentioned above, this study selected 25°C as the reference for a comfortable temperature, both for the ambient room temperature and the temperature at the occupancy point.

Statistical Analysis of Cooling Performance and Energy Consumption

Before comparing the experimental configurations, a factorial analysis of variance (ANOVA) was conducted to examine the effects of compressor technology, indoor installation height, fan speed, workstation layout, and the interactions between these variables on cooling performance and energy consumption. All 32 observations in the Displacement configuration failed to achieve a comfortable room temperature of 25°C within the 60-minute observation period. These observations were not assigned a time-to-comfort value and were excluded from the factorial analysis of this response variable.

For energy consumption, the full factorial analysis included all 96 observations. The results showed that compressor technology and indoor-unit installation height had a statistically significant effect on energy consumption ($p < 0.001$), with large effect sizes (partial $\eta^2 = 0.999$ and 0.995, respectively). These findings indicate that compressor type and installation height are the dominant factors influencing electricity consumption under these experimental conditions. The effects of fan speed and workspace layout were statistically significant in the factorial ANOVA; however, the Kruskal–Wallis test did not support these effects, so they should be interpreted with caution. A significant interaction between compressor technology and installation altitude was also identified ($p < 0.001$), indicating that the effect of installation altitude on energy consumption depends on the compressor type. This finding supports the interpretation that a cooling system's performance cannot be evaluated based on compressor technology or airflow distribution in isolation, but must also account for their interaction.

For the time required to reach the target temperature, the factorial ANOVA was restricted to the PM_Above and PM_Middle configurations ($n = 64$). The analysis revealed statistically significant differences between the tested factors and their interactions ($p < 0.001$). However, these results were interpreted alongside the descriptive data, as temperature measurements were recorded at 2-minute intervals, resulting in limited variation within treatments for most configurations.

The Effect of Installation Height on Cooling Performance and Energy Consumption

The effect of installation height on cooling performance in non-inverter air conditioners

This sub-section will discuss the effect of the installation height of indoor air-conditioning units on the time required to reach a comfortable temperature. All the results of the experiments in this sub-section are shown in Figure 5 for non-inverter air-conditioners and Figure 6 for inverter air-conditioners.

For all NI_PMA configuration variants, the chamber temperature decreased consistently from the start of the test. The initial temperature ranged from 29.0-29.4°C, then decreased between the 10th and 15th minutes. At the 10-minute mark, the temperature ranged from 25.0-25.2°C. It then dropped to 24.0-24.4°C by the 20-minute mark. After approximately 30 minutes, the temperature approached a more stable state, ranging from 23.5 to 23.7 °C. At the end of the test, at the 60th minute, the temperature ranged from 22.8 to 23.2 °C. Among the NI_PMA configuration variants, NI_PMA_F4_MD and NI_PMA_F2_MD reached lower final temperatures compared to the other variants.

The temperature in the NI_PMM configuration also decreased to 25°C at the 10th minute. The temperature then ranged from 23.1 to 23.5°C between the 20th and 24th minutes. By the 26th minute, temperature fluctuations became more noticeable, particularly in the F4_SD and F4_MD variants. F4_SD rose to the range of 24.6-24.7°C between the 28th and 30th minutes before declining again. F4_MD also fluctuated, rising to about 24.8°C at the 38th minute, with fluctuations continuing until the end of the test. F2_SD remained relatively stable after the 30th minute, staying within the range of 22.8-23.2°C. F2_MD showed fluctuations in the second half of the test, with the temperature reaching a range of 24.8-24.9°C at minutes 48-50. In the NI_D_Bottom configuration, the temperature dropped only to 28.0–28.2 °C during the first 10 minutes. Subsequently, the temperature remained between 27.5 and 28.1 °C from the 14th to the 20th minute. After the 20th minute, the temperature fluctuated between 27–28 °C. Among the configuration variants, NI_D_Bottom_F4_SD shows the lowest temperature, occasionally reaching 26.5–26.8 °C. NI_D_Bottom_F2_MD exhibits the highest temperature, ranging from approximately 27.8–28.2 °C for most of the test period. At the 60th minute, the temperature remained within the range of 26.5–27.9°C.

All three configurations showed different temperature-decline patterns from the start of the test. NI_PMA showed the most consistent decline. Its temperature dropped from 29.0–29.4 °C at the start of the test to the range of 22.8-23.2 °C at the 60th minute, with no significant fluctuations after the 30th minute. NI_PMM also decreased in the early phase, reaching 23.1-23.5°C between the 20th and 24th minutes, after which the temperature rose again to 24.6-24.9°C. The NI_D_Bottom configuration exhibited a different pattern from the other two configurations. Its temperature fluctuated between 27 and 28 °C from the start until the 20th minute. The final temperature for NI_D_Bottom remained within the range of 26.5-27.9 °C.

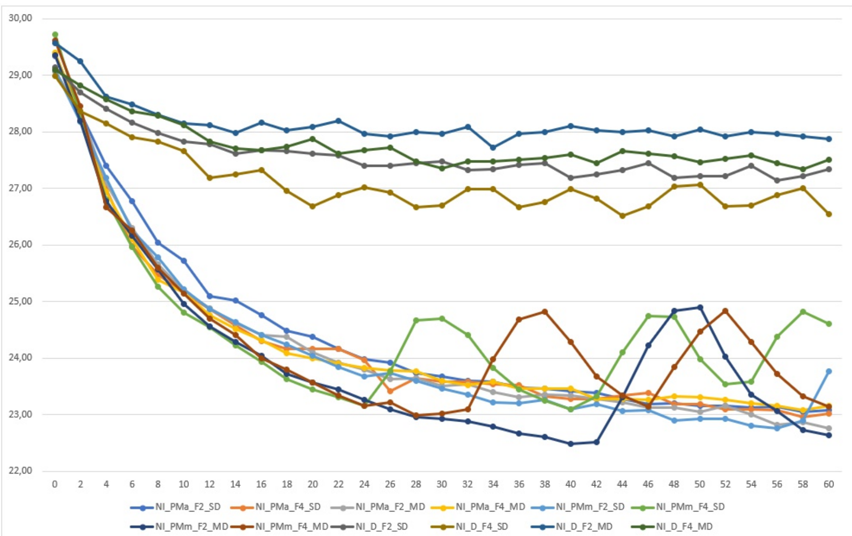

Figure 5. Time series temperature scatter plot graph of non-inverter air conditioners

The effect of installation height on cooling performance in inverter air conditioners

The temperature decrease in the I_PMA configuration occurred from minute 0 to minute 16. By minute 16, the room temperature had dropped to 24.9°C. The I_PMa_F2_SD variant configuration decreased from approximately 29.1°C to approximately 25.3°C by minute 16. The temperature then fluctuated between 24.4–25.3°C. Meanwhile, I_PMa_F4_SD showed a gradual temperature decrease from 29.0°C to approximately 25.4°C by minute 16. The temperature then stabilized between 24.7 and 25.2°C. A different pattern was observed in I_PMa_F2_MD, which recorded a minimum temperature of 24.3°C at the 26th minute. After 30 minutes, all configurations showed relatively small temperature fluctuations. During the 30–60-minute period, the room temperature generally ranged from 24.4 to 24.9°C. The I_PMa_F2_MD configuration recorded a final temperature of approximately 24.3°C.

In the I_PMm configuration, the temperature decreased from the 2nd to the 12th minute, dropping from 29°C to 24.7–25.3°C. In the I_PMm_F2_SD configuration variant, the temperature decreased from 29.3°C to 24.9°C at the 14th minute. The temperature then fluctuated between 25.0–25.7°C. Meanwhile, I_PMm_F4_SD dropped to 24.9°C at minute 12. The temperature then fluctuated between 24.9–25.8°C. In the I_PMm_F2_MD variant configuration, the temperature decreased relatively consistently in the early phase, reaching approximately 24.7°C between the 12th and 14th minutes. After that, the temperature fluctuated, reaching a low of 24.4°C at the 54th minute. In the I_PMm_F4_MD configuration, the temperature dropped to 24.8°C at the 18th minute. The temperature then fluctuated between 24.8–25.7°C. From the 12th to the 18th minute, all configurations exhibited a fluctuating pattern of temperature decline, indicating that conditions were beginning to stabilize. During the 20–60-minute period, all configurations generally remained within the 24.4–25.8 °C range.

The temperature drop in the I_D_Bottom configuration differed from that of the other two configurations. The I_D_Bottom_F2_SD configuration experienced a temperature drop in the initial phase, from about 29.5°C to about 27.2°C at the 12th minute. A different pattern was observed in I_D_Bottom_F4_SD, which dropped to 26.8°C at the 12th minute. The temperature then rose and fluctuated between 26.6–27.3°C. Meanwhile, I_D_Bottom_F2_MD dropped from approximately 29.6°C to approximately 28.1°C at the 12th minute. This temperature then stabilized between 27.7–28.1°C. I_D_Bottom_F4_MD decreased from approximately 29.7°C to approximately 27.8°C at the 14th minute. This temperature tended to stabilize within the 27.5–27.8 °C range. From the 12th minute to the 16th minute, the temperature in all I_D_Bottom configurations entered a fluctuating phase; by the end of the observation (the 60th minute), the temperature ranged from 27.2–27.5°C in all configurations.

The I_PMa configuration showed the fastest temperature drop, reaching 24.9°C at the 16th minute and stabilizing in the range of 24.4–24.9°C until the 60th minute. The I_PMm configuration showed a temperature drop over a nearly identical time span, from the 12th to the 18th minute, but with a slightly higher final temperature, ranging from 25.2 to 25.5°C. In contrast, I_D_Bottom showed a slower

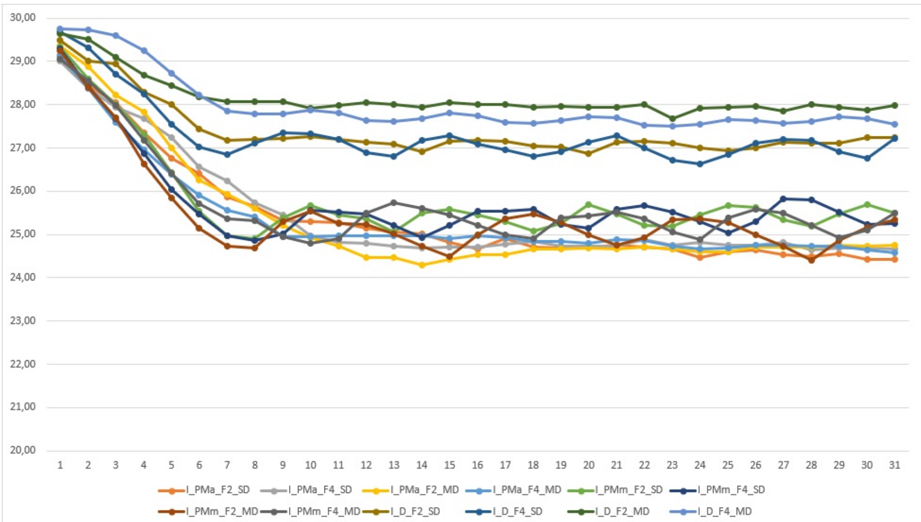

Figure 6. Time series temperature scatter plot graph of inverter air conditioners

temperature decrease in the initial phase, with temperatures between the 12th and 14th minutes still ranging from 26.8 to 28.1°C. The final temperature in the I_D_Bottom configuration was also the highest compared to I_PMa and I_PMm, ranging from 27.2 to 27.5°C.

A comparison of the three configurations shows that the rate of temperature decline is directly proportional to the installation height at the PMa and PMm levels. In contrast, the I_D_Bottom configuration consistently produces higher room temperatures throughout the observation phase. The fluctuation patterns following the initial cooling phase also differ among these configurations. I_PMm exhibited a wider range of fluctuations than I_PMa, whereas I_D_Bottom exhibited the narrowest final range of fluctuations among the three. These differences indicate that, in addition to influencing the initial cooling rate, configuration position also contributes to temperature stability in subsequent phases.

Comparison of the effect of installation height on cooling performance in non-inverter and inverter air conditioners

The NI_PMa configuration showed a continuous decrease in temperature until the end of the test, from 29.0–29.4 °C at the start of the test to 22.8–23.2 °C at the 60th minute. The I_PMa configuration also decreased in the early phase from 29.0–29.1 °C, but its temperature stabilized more quickly in the range of 24.4–24.9 °C from the 16th to the 60th minute. Meanwhile, the NI_PMm configuration dropped to the range of 23.1–23.5 °C between the 20th and 24th minutes, before some of its variants fluctuated upward to the range of 24.6–24.9 °C in the second half of the test. The I_PMm configuration showed a different pattern, with its temperature dropping to 24.7–25.3°C between the 12th and 18th minutes, then fluctuating within 24.4–25.8°C until the 60th minute. The NI_D_Bottom configuration only decreased to the range of 28.0–28.2°C during the first 10 minutes, then fluctuated within the range of 27–28°C after the 20th minute, and remained within the range of 26.5–27.9°C at the 60th minute. The I_D_Bottom configuration showed a similar pattern, with the temperature decreasing to 26.8–28.1°C between the 12th and 14th minutes, then stabilizing at 27.2–27.5°C at the 60th minute.

This comparison shows that the temperature difference between NI and I is most pronounced in the PMa and PMm configurations, with NI reaching a final temperature approximately 1.6–2.6°C lower than I in both configurations. In the PMa configuration, NI_PMa exhibited significant fluctuations after the 30th minute, whereas I_PMa had reached a steady state as early as the 16th minute, indicating that I_PMa stabilized more quickly. In the PMm configuration, both configurations exhibited fluctuations in the second half of the test; however, the fluctuation range of I_PMm (24.4–25.8°C) was higher than that of NI_PMm (23.1–24.9°C). Unlike PMa and PMm, the D_Bottom configuration showed a smaller final temperature difference between NI and I, with both configurations exhibiting a fluctuation pattern without a decline after the initial cooling phase.

The Effect of Installation Height on Energy Consumption

This sub-section will discuss the effect of the installation height of indoor air-conditioning units on energy consumption. All the results of the experiments in this sub-section are shown in Figure 7 for non-inverter air-conditioners and Figure 8 for inverter air-conditioners.

The effect of installation height on energy consumption in non-inverter air conditioners

In the NI_PMa configuration, power consumption increased from the start of the measurement period, reaching 880–920 watts by the 4th minute. This increase occurred in all configuration variants, though at varying rates. Power consumption in the NI_PMa_F2_SD configuration rose gradually from approximately 760 watts at the 2nd minute to 920–930 watts in the subsequent phase. Power consumption then stabilized in the 910–930 watt range, with minor fluctuations. In the NI_PMa_F4_SD configuration variant, the initial power consumption of 880 watts increased to 930–950 watts in just 2 minutes. Power consumption then fluctuated within a consistent range of 930–960 watts. The NI_PMa_F2_MD configuration exhibited a different pattern. Power briefly rose to 920–930 watts in the initial phase, then gradually decreased through the end of the observation period.

NI_PMa_F4_MD recorded the highest spike among the four configuration variants. Its power consumption reached approximately 950 watts at the 2-minute mark. This power consumption then stabilized at 970–980 watts. After the 20-minute mark, fluctuations in NI_PMa's power consumption decreased across all configuration variants, compared to the spikes observed in the initial phase. Power consumption remained between 880 and 980 watts during the 30–60-minute period. All four configuration variants exhibited a similar pattern throughout the test period: a rapid increase in the initial phase, followed by a stable condition with minor fluctuations. Among the four configurations, NI_PMa_F4_MD recorded the highest power consumption and the smallest fluctuation range, at approximately 970–980 watts. In contrast, NI_PMa_F2_MD exhibited the widest fluctuation range, with power continuing to decrease until it reached a low of approximately 880–890 watts at the end of the observation.

Energy consumption in the NI_PMm configuration also increased from the start of the measurement, then stabilized around the 4th minute, as shown in Figure 12. At the 4th minute, all configuration variants were in the 810–890 watts range. NI_PMm_F4_MD recorded the highest value during the initial phase, at 890.11 watts. In the NI_PMm_F2_SD configuration, power increased from about 850 watts at the 2-minute mark to the 925–930-watt range in the following period. It then stabilized in the 890–930-watt range until the 56th minute. At the 58th minute, power consumption dropped to 21.80 watts. In the NI_PMm_F4_SD configuration, there was a gradual increase from approximately 850 watts to 890–900 watts by the 22nd minute. Power then decreased between the 24th and 26th minutes before rising again to approximately 950 watts by the 28th minute. The NI_PMm_F2_MD configuration exhibited a different pattern. Power increased gradually from about 760 watts at the 2-minute mark and reached about 890 watts at the 12-minute mark. It then stabilized in the 880–900-watt range before decreasing at the 42–44-minute and 50-minute marks.

In NI_PMm_F4_MD, the power at the 2-minute mark was 860 watts and increased to 925–930 watts between the 12th and 16th minutes. This power then remained relatively stable, dropping at minutes 32-34 and 44-50. Between minutes 12 and 40, most configuration variants showed stable power in the range of 880-930 watts, accompanied by some fluctuations. The power drops in these configurations were temporary. During the period from the 40th to the 60th minute, fluctuations occurred in all configurations. NI_PMm_F4_MD recorded high energy consumption, around 920-930 watts. NI_PMm_F2_MD remained within the 870–890-watt range until the end of the measurement. All four configurations exhibited a similar pattern: an increase in the initial phase, followed by a relatively stable condition interspersed with several temporary drops. Among the four configurations, NI_PMm_F4_MD recorded the highest and most stable energy consumption, at approximately 920–930 watts. In contrast, NI_PMm_F2_MD recorded the lowest value at the end of the observation, at approximately 870-890 watts.

Energy consumption in the NI_D_Bottom configuration remained high throughout the observation period compared to the two previous configurations. Power consumption ranged from 800 to 950 watts, with greater fluctuations. NI_D_Bottom_F4_MD consistently recorded the highest peak values among the other NI_D_Bottom configurations in nearly every measurement. Power reached approximately 940–950 watts during several measurement periods, particularly at the 8th, 24th, 42nd, and 58th minutes. From the 2nd to the 60th minute, a recurring pattern observed across all configuration variants was a rise in power to the 800–950-watt range, lasting 2 to 4 minutes. After the increase, power dropped to 20–30 watts, followed by another rise in the subsequent period.

NI_D_Bottom_F2_SD and NI_D_Bottom_F2_MD show an up-and-down pattern with peak values that are close together, in the range of 830-930 watts. NI_D_BOTTOM_F4_SD recorded lower peaks, around 780 watts at the 52-minute mark and 825 watts during the 44-46-minute period. Toward the end of the observation period, particularly during the 56-60-minute period, high peaks were observed in the range of 850-940 watts. This fluctuation pattern continued until the end of the observation period.

All three configurations (NI_PMA, NI_PMM, NI_D_Bottom) exhibited different energy consumption patterns after the initial ramp-up phase. NI_PMA remained within the range of 880-980 watts with minor fluctuations throughout the observation period. NI_PMM remained within the range of 870–930 watts under steady-state conditions, but was interspersed with several temporary drops of up to 21.80 watts. NI_D_Bottom had the highest range among the three configurations, namely 800-950 watts, but with a consistently recurring pattern of ups and downs throughout periods 2 through 60. Power consumption rose to its peak range for 2–4 minutes before dropping to 20-30 watts.

This comparison shows that energy consumption varies among the three configurations, although their peak ranges are relatively close. NI_PMa exhibits the most stable pattern without any sharp drops, while NI_PMm shows a steady pattern interspersed with sharp drops in some configuration

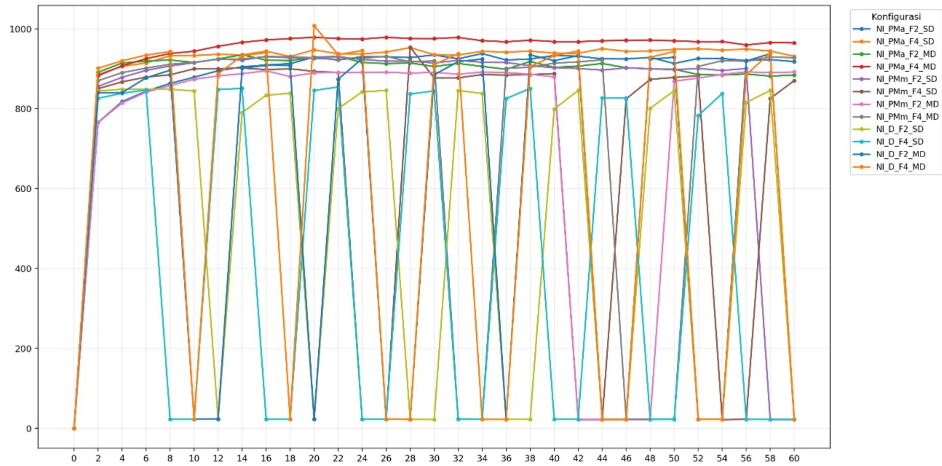

Figure 7. Energy consumption of non-inverter air conditioners

variants. NI_D_Bottom exhibits a recurring pattern of ups and downs. Across the entire observation period, the F4_MD variant consistently recorded the highest peak values (NI_PMa_F4_MD at 970–980 watts, NI_PMm_F4_MD at 920–930 watts, and NI_D_Bottom_F4_MD at 940–950 watts), indicating that the F4_MD variant contributes to the highest energy consumption regardless of its primary configuration type.

The effect of installation height on energy consumption in inverter air conditioners

Energy consumption in the I_PMA configuration increased from the 4th to the 16th minute, then all configurations decreased and stabilized in the subsequent phase. From the 4th minute to the 12th minute, all configuration variants remained within the range of 480-680 watts. In the I_PMA_F2_SD configuration variant, power consumption increased from 530 watts at minute 4 to 570 watts at minute 8. Power then decreased, reaching 350-360 watts between minutes 16 and 26, before stabilizing through the end of the observation period. I_PMA_F4_SD recorded the most significant increase in the early phase, from about 680 watts at the 6th minute, then peaking at 760 watts at the 16th minute. Power then gradually decreased to about 380 watts between the 28th and 30th minutes, before stabilizing in the 370-390-watt range.

In the I_PMA_F2_MD configuration, power consumption initially was 490 watts at the 4-minute mark, then dropped to about 450 watts at the 6-minute mark. Power consumption increased to about 715 watts at the 16-minute mark. Subsequently, power consumption gradually decreased to about 340 watts between the 32nd and 34th minutes. In the I_PMA_F4_MD configuration, power consumption was about 530 watts at the 4th minute and rose to 580 watts at the 12th minute. Subsequently, power consumption gradually decreased to the 380–400-watt range between the 20th and 30th minutes, before stabilizing with slight fluctuations until the end of the observation period. After the 30th minute, most configurations showed stable power in the 340–400-watt range, although minor fluctuations remained in each configuration. From the 32nd to the 36th minute, I_PMA_F2_MD showed lower power, ranging from 335 to 360 watts, before increasing again and stabilizing in the 350-370-watt range until the end of the observation.

From the 48th minute to the 60th minute, fluctuations reappeared in all I_PMA configuration variants. In I_PMA_F2_SD, power consumption increased to 400 watts between the 50th and 58th minutes, while I_PMA_F4_MD reached approximately 410 watts at the 60th minute. At the end of the observation, all I_PMA configuration variants showed similar values, ranging from 360 to 410 watts. Hence, the differences between configurations were smaller than in the early phase of the observation, with I_PMA_F4_MD and I_PMA_F2_SD recording slightly higher values than the other configurations.

Power consumption in the I_PMm configuration also remained steady from the 2nd to the 4th minute, before fluctuating and gradually decreasing toward a more stable state, as shown in Figure 15. In the fourth period, all I_PMM configurations (F2_SD, F4_SD, F2_MD, F4_MD) reached their first peak in the range of 460–485 watts. Power then decreased in the sixth minute, particularly for I_PMm_F4_SD, which dropped to about 310 watts. In the 8th minute, all configurations rose again, forming a second peak of 370–420 watts before gradually declining through the 12th period. After the 12th period, the power for all configurations decreased. I_PMm_F2_SD and I_PMm_F2_MD dropped to about 16 watts in the 14 minutes, while I_PMm_F4_SD and I_PMm_F4_MD remained in the 260-watt range.

Toward the end of the observation period, between the 56th and 60th minutes, power consumption across the four I_PMM configuration variants returned to a nearly identical range, namely around 250–310 watts. This condition showed a more stable pattern than the early phase of the observation. Overall, this configuration exhibited three main phases. The first phase consisted of an increase and fluctuations during periods 2 through 12. The second phase involved a gradual decrease in power accompanied by repeated ups and downs during the 12th to 20th minutes. The third phase was relatively stable, with repeated fluctuations within the 250–300-watt range from the 20th to the 60th minute.

Power consumption across all I_D_Bottom configurations also increased from the start of the observation, specifically from the 2nd period to the 4th period, as shown in Figure 16. The four I_D_Bottom configuration variants rose from approximately 17–22 watts to 555–600 watts. In the I_D_Bottom_F4_MD configuration variant, power consumption rose again at the 8-minute mark, forming a second peak of approximately 575 watts. The other three I_D_Bottom configuration variants decreased gradually between the 8th and 10th minutes.

In the I_D_Bottom_F4_MD configuration variant, power consumption dropped to 103 watts at the 10-minute mark. The I_D_Bottom_F2_SD, I_D_Bottom_F4_SD, and I_D_Bottom_F2_MD configurations remained within the 380–530-watt range during the same period. From the 14th period until the end of the observation at the 60th period, the four I_D_Bottom configuration variants exhibited a repeating pattern of rises and falls. The power rose to the 350–460-watt range, then dropped below 100 watts; however, this drop occurred alternately among the configuration variants, not simultaneously across all four. Among the four configurations, I_D_Bottom_F4_SD recorded the highest peak values in many periods, including around 460 watts in periods 28 and 38. I_D_Bottom_F2_MD showed the most frequent drops throughout periods 14 through 60, with values repeatedly falling below 100 watts.

Toward the end of the observation period, specifically between the 52nd and 60th minutes, all four configuration variants exhibited peak values that were close to one another, ranging from 350 to 455 watts. Overall, these configurations exhibited two main phases. The first phase consisted of an increase and fluctuations during the 0th to 14th minute. The second phase was a repeating pattern with peak values in the range of 350–460 watts, interspersed with alternating decreases among the configurations, lasting from the 14th to the 60th minute.

The three configurations (I_PMA, I_PMM, I_D_Bottom) showed varying energy consumption during the initial and final phases of the observation. I_PMA recorded the highest initial peak value of 760 watts for the I_PMA_F4_SD configuration variant, then stabilized in the 360–410-watt range. I_PMM reached an initial peak in the 460–485-watt range, then stabilized at a lower range of 250–310 watts, and subsequently dropped gradually below 100 watts. I_D_Bottom recorded the highest initial peak among the three configurations, at 555–600 watts, and stabilized in the 350–455-watt range by the end of the observation, which was also accompanied by periodic drops to below 100 watts for each configuration variant. This comparison shows that I_D_Bottom maintains the highest final

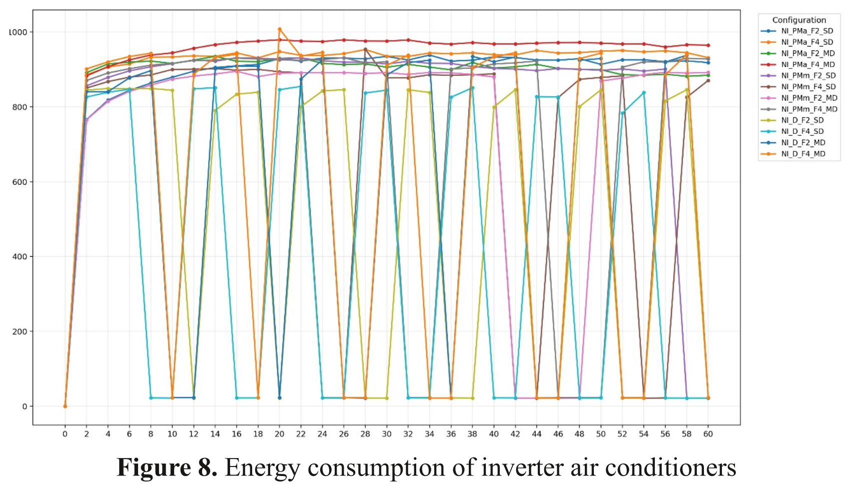

Figure 8. Energy consumption of inverter air conditioners

power range among the three configurations. I_PMA does not exhibit the up-and-down cycles seen in I_PMm and I_D_Bottom.

Comparison of the Effect of Installation Height on Energy Consumption in Non-Inverter and Inverter Air Conditioners

Configurations of NI and I with the same variants show significantly different energy consumption levels. NI_PMa stabilizes in the high range, namely 880-980 watts, while I_PMA stabilizes in a much lower range, namely 360-410 watts, after a gradual decline from an initial peak of 760 watts. NI_PMm stabilized in the 870-930-watt range with temporary sharp drops at several points, while I_PMm stabilized in a lower range, namely 250-300 watts, accompanied by a recurring pattern of periodic drops below 100 watts throughout the observation period. NI_D_Bottom exhibited a recurring up-and-down pattern within a peak range of 800-950 watts, whereas I_D_Bottom showed a similar recurring up-and-down pattern, but within a lower peak range of 350-460 watts.

This comparison shows that Configuration I consistently operates at a lower energy consumption level than Configuration NI in the same variant, with the peak range difference reaching more than half that of NI. The recurring up-and-down pattern with drops approaching zero is also more pronounced in Configuration I, particularly in I_PMm and I_D_Bottom, compared to NI_PMm, which only experiences a temporary sharp drop. The closest similarity in patterns between the two configuration groups was observed in the D_Bottom variant, where both NI_D_Bottom and I_D_Bottom exhibited a recurring up-and-down pattern throughout the observation period, albeit at different power levels.

The Interaction Between Compressor Technology and Airflow Distribution

The interaction between compressor technology and airflow distribution in non-inverter air conditioners

This sub-section discusses the interaction between compressor technology and airflow distribution in non-inverter air conditioners. All experimental results in this sub-section are shown in Figure 9.

In the NI configuration, power consumption in the NI_PMa_F2_SD variant rose rapidly to the 900–930-watt range within the first 10 minutes, then remained at that high level until the 58th minute, before dropping at the 60th minute. In this configuration variant, the temperature decreased smoothly and consistently from approximately 29.2°C to approximately 23.0°C, with no significant spikes throughout the test. A similar pattern was observed in NI_PMa_F4_SD, F2_MD, and F4_MD, with power rising rapidly to the 900–980-watt range and remaining at that high level for 60 minutes without any shutdown cycles. The temperature in these three NI_PMA configurations decreased steadily from approximately 29°C to approximately 23°C, indicating that the compressor operated continuously without interruption until the end of the observation.

The NI_PMm configuration shows variations in on/off cycles across its variants. The NI_PMm_F2_SD maintains power within the 900–930-watt range until the 56th minute, before dropping at the 58th minute. The temperature in this variant decreases consistently from 29°C to approximately 22.8°C, with a slight increase at the end of the test when the power is turned off. NI_PMm_F4_SD exhibits a repeating on/off cycle pattern, with power rising to about 900 watts, stabilizing for several minutes, then dropping at the 24th, 40th–42nd, and 54th–56th minutes. Each time the power was cut off, the temperature in this variant rose back to the 24.7–24.8°C range before dropping again when the compressor turned on. Meanwhile, NI_PMm_F2_MD maintained a high power level until the 40th minute, then dropped in power consumption between the 42nd and 48th minutes before rising again. The temperature in this variant drops to around 22.7°C before the 40th minute, then rises again to around 24.9°C. NI_PMm_F4_MD experiences two drops in power consumption: between the 32nd and 34th minutes and between the 46th and 50th minutes. The temperature in this variant rose again to about 24.8°C during each power-consumption drop.

All variants in the NI_D_Bottom configuration exhibited a pattern different from the other configurations, namely, very frequent on-off cycles throughout the 60-minute test. The power in these four configuration variants rose to 800–950 watts, then dropped repeatedly at short intervals of about 8–10 minutes per cycle, more frequently than in the NI_PMm configuration. The temperature in all NI_D_Bottom variants fluctuated within a narrow range of 26.5–29.5°C and never dropped as low as in the NI_PMa or NI_PMm configurations. Each time the compressor was turned on, the temperature dropped slightly, then rose again when the compressor was turned off, forming a consistent sawtooth pattern from the beginning to the end of the test. NI_D_F4_MD recorded the highest initial temperature, approximately 29.6°C, but still

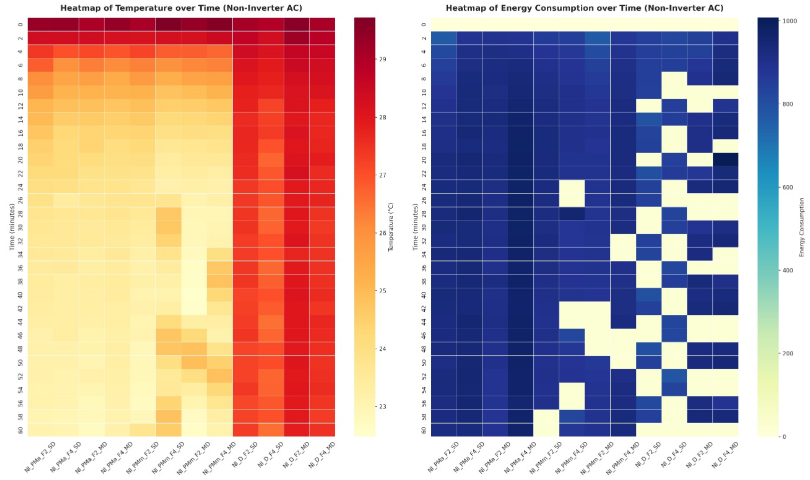

Figure 9. Heatmap of temperature and energy consumption in non-inverter air conditioners

followed a cyclic pattern similar to the other variants, with the final temperature ranging from 27.3–27.5°C.

All three NI configurations exhibit different relationships between power consumption patterns and temperature changes. NI_PMa exhibits consistently high power consumption without any on-off cycles, which aligns with the most consistent temperature decrease without any significant rebound. NI_PMm shows variation among its variants, with some variants maintaining high power consumption until the final minutes and others exhibiting on-off cycles accompanied by a temperature rebound of 24.7–24.9°C. NI_D recorded the highest on/off cycle frequency among the three configurations, with the shortest cycle intervals (8–10 minutes) and the narrowest yet highest temperature fluctuation range (26.5–29.5°C) compared to NI_PMa and NI_PMm.

The interaction between compressor technology and airflow distribution in inverter air conditioners

This sub-section discusses the interaction between compressor technology and airflow distribution in inverter air conditioners. All experimental results in this sub-section are shown in Figure 10.

Power consumption at I_PMa fluctuated during the initial phase from minute 0 to minute 15, briefly reaching the 500–770 watt range. After that phase, power decreased and stabilized at a low level in the 355–400-watt range until the end of the test, without any sudden drops. The temperature decreased smoothly and continuously from approximately 29°C to 24.5–25°C, without any significant rebound, in line with the uninterrupted power pattern. The F4_SD and F2_MD variants, which recorded the highest peak power in the 700–770-watt range, reached a slightly lower final temperature around 24.5°C compared to the F2_SD and F4_MD variants, which were in the 24.7–25°C range. This pattern indicates that the airflow in the I_PMa configuration is distributed continuously and evenly throughout the room, rather than being concentrated at the sensor location. This condition prevents the temperature from rising again even after power decreases to a low steady-state level, because the cool-air distribution is sufficiently even.

In contrast to the pattern observed in I_PMa, the four variants in I_PMm exhibited frequent, repetitive on/off cycles throughout the test, with lower peak power ranging from 250 to 480 watts. The temperature fluctuated within a narrow range of 24.8–29°C, following the pattern of these power fluctuations, dropping rapidly in the initial phase and then continuing to fluctuate without ever settling permanently at a low level. The F2_MD and F4_MD variants exhibited slightly higher peak power (300–325 watts) than the F2_SD and F4_SD variants (250–270 watts) during subsequent cycles. Nevertheless, the oscillation patterns remained similar across all variants.

The I_D_Bottom configuration again exhibits a different pattern. All four variants, F2_SD, F4_SD, F2_MD, and F4_MD, show very frequent on/off cycles throughout the 60-minute test, with power rising to a peak in the 400–600-watt range and then dropping repeatedly in short intervals of about 8–10 minutes per cycle. Temperatures across all variants dropped rapidly during the initial phase (minutes 0 through 10), then immediately entered a phase of minor fluctuations within a narrow range of 26.5–29.5°C, following the repetitive rise-and-fall pattern of power. The F4_SD and F4_MD variants, with higher airflow, showed slightly higher power peaks in the initial phase, indicating that the compressor was working harder to move a larger volume of air. Nevertheless, the subsequent cycle pattern remained similar to that of the F2 variant; see the figure. The very frequent on/off cycling in this configuration indicates that the cold airflow rapidly cools the sensor area locally, causing the compressor to reduce power before the air has a chance to distribute evenly throughout the room. As a result, the overall room temperature never stabilizes at a consistently low level.

The three configurations in Type I exhibit different relationships between power consumption patterns and temperature distribution. I_PMa shows a transition from high power to a steady-state low power level without a temperature rebound, indicating uniform air distribution. I_PMm exhibits a consistent on/off cycle at a medium peak power level (250–480 watts), accompanied by temperature fluctuations that never settle at a low level. I_D_Bottom exhibits the highest on/off cycle frequency with the shortest intervals (8–10 minutes) among the three configurations, as well as the narrowest range of temperature fluctuations, though at the highest level (26.5–29.5°C) compared to I_PMa and I_PMm.

Comparison Between Compressor Technology and Airflow Distribution in Non-Inverter and Inverter Air Conditioners

The NI_PMa configuration maintained high power consumption (900–980 watts) without any shutdown cycles throughout the 60-minute test, with a consistent drop in temperature and no rebound. The I_PMa configuration exhibited a different pattern, with power fluctuating in the initial phase (500–770 watts) before dropping and stabilizing at a low level (355–400 watts) until the end of the test; however, the temperature continued to decrease smoothly without a rebound, as seen in the NI_PMa configuration. In the PMm configuration, NI_PMm exhibited variations among variants, with some variants maintaining high power (900–930 watts) until the final minutes and others showing on/off cycles at the same power level, accompanied by a temperature rebound to 24.7–24.9°C. The I_PMm configuration also exhibited on/off cycling across all variants, but at a much lower power level, specifically in the 250–480-watt range. Meanwhile, both the NI_D_Bottom and I_D_Bottom configurations exhibited very frequent on/off cycling patterns with short intervals of about 8–10 minutes per cycle throughout the test, with NI_D_Bottom recording peak power in the 800–950-watt range and I_D in the 400–600-watt range.

This comparison shows that in the PMa configuration, the AC type has a significant impact on power consumption patterns but not on temperature drop patterns: NI_PMa requires a continuously high power input to achieve a consistent temperature drop, whereas I_PMa achieves an equivalent temperature drop pattern with only a low steady-state power input after the initial phase, indicating better cold air distribution efficiency in I_PMa despite its significantly lower power consumption. In the PMm configuration, both AC types exhibit on/off cycles, but at significantly different power levels (900–930 watts for NI_PMm versus 250–480 watts for I_PMm), while temperature rebound patterns still occur in both types, indicating that the on/off cycles in PMm occur regardless of the amount of power used. Unlike PMa and PMm, the D_Bottom configuration shows similar on/off cycle patterns between NI and I in frequency and interval, with the main difference in peak power magnitude: NI_D_Bottom records significantly higher power than I_D_Bottom to achieve a comparable temperature fluctuation pattern.

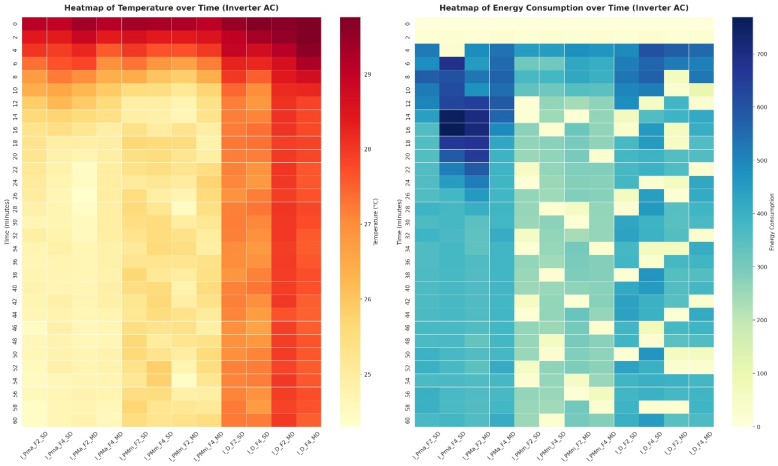

Figure 10. Heatmap of temperature and energy consumption in non-inverter air conditioners

This pattern indicates that the difference in efficiency between NI and I is most pronounced in the PMa configuration. In contrast, in the PMm and D_Bottom configurations, the on/off cycle characteristics are more influenced by the installation position than by the type of compressor used.

Comparison of the Effect of Installation Height on Temperature at the Occupancy Point

This research indicates that a sudden drop in room temperature does not always result in an ideally comfortable environment in the occupied zone. In the PM_Above configuration, for example, although the average room temperature has reached the target temperature, the temperature in the occupants' activity areas remains relatively high. This indicates that high cooling capacity does not automatically result in thermal comfort if cool air is distributed ineffectively within the room.

It is hypothesized that this situation is linked to the airflow pattern created by installing the indoor unit at a height of 2.6 meters, as air discharged from the unit moves along the ceiling surface before gradually descending as its momentum decreases. As a result, cold air predominantly circulates in the upper layer of the room and takes longer to reach the occupied zone. This results in greater thermal stratification, meaning that while the average room temperature may reach the target value, areas where occupants are active still do not receive adequate cooling. These findings suggest that an air-conditioning system's performance should not be evaluated solely on average room temperature, but also on temperature distribution in occupied zones, which is the primary indicator of thermal comfort. A limitation of this study is that it did not collect vertical air-velocity profile data, which would be required to empirically confirm this airflow mechanism. Future research should include such measurements to validate this hypothesis.

Conversely, lowering the unit's installation height to the PM_Middle setting results in more effective air distribution towards the occupants' activity zone. In this configuration, the air takes a shorter path to

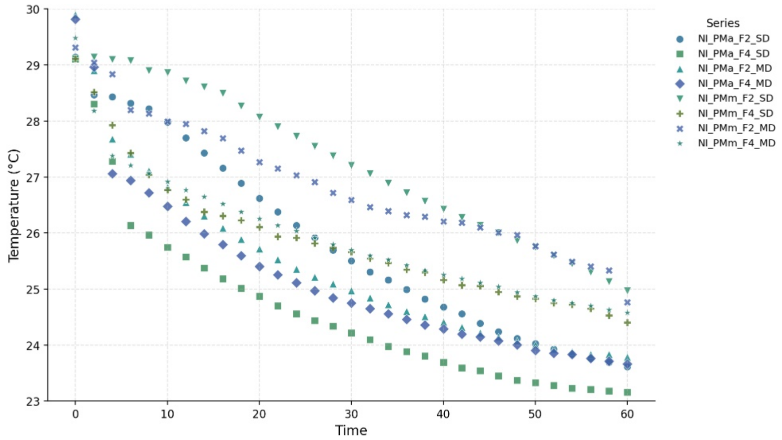

Figure 11. Time series temperature fluctuations of a workdesk with a non-inverter air conditioner

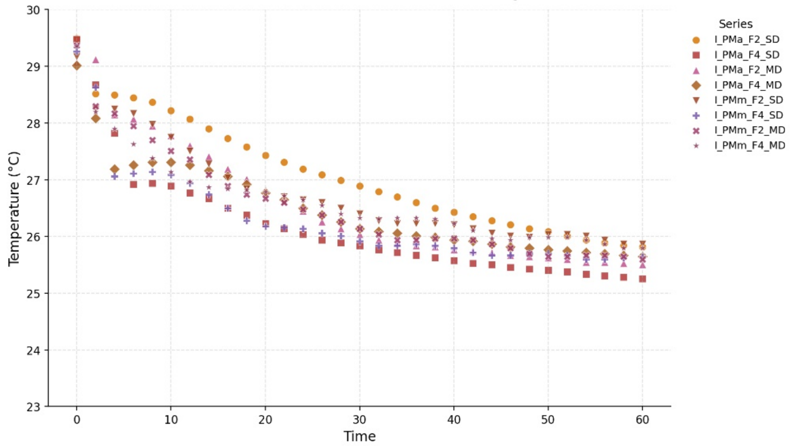

Figure 12. Time series temperature fluctuations of a workdesk with an inverter air conditioner

reach the occupied zone. As a result, air mixes more quickly, and the temperature distribution becomes more uniform (see Figures 11 and 12). The difference in the time taken to reach the target temperature between the two compressor technologies also becomes smaller. This indicates that optimizing air distribution can reduce the influence of compressor operating characteristics on cooling performance. In other words, the effectiveness of air distribution plays a role just as important as compressor technology in determining the performance of an air-conditioning system (Heidarinejad et al., 2015).

Optimal Configuration for Residential Use

The research findings indicate that the correlation between cooling rate, energy efficiency, and thermal conditions in occupied areas is complex and non-linear. A change in one factor does not necessarily change the others; therefore, no single configuration can achieve optimal performance across all parameters tested. These results indicate that, to evaluate the performance of an air-conditioning system, you must consider multiple factors, including thermal comfort, energy consumption, and thermal conditions within the occupied zone.

The key difference between inverter and non-inverter air conditioners lies in how compressor technology interacts with the indoor unit's installation configuration. Most non-inverter air conditioners cool faster because their compressors run continuously until the set temperature is reached, unlike inverter air conditioners. Inverter air conditioners, by contrast, provide a more gradual cooling response through the commutation process (Almogbel et al., 2020), which continuously adjusts the compressor's capacity. These technological features are highly functional and deliver excellent performance across various metrics.

These findings can be applied when selecting an efficient air conditioning system for the home. Using the PM_Middle configuration with a non-inverter AC is more practical for achieving comfort in rooms that are used only occasionally or for short periods. A cooling time of about 10 minutes is the most suitable result. The PM_Middle configuration with an inverter AC is better suited for long-term use in rooms (living rooms, home offices) or bedrooms, as it offers thermal comfort and requires less energy.

By utilizing compressor control, inverter air conditioners maintain the unit's temperature by operating at low power for extended periods. This is achieved by avoiding frequent on-off cycles, which helps maintain the system's temperature stability while reducing fluctuations in electrical load and cumulative energy consumption. Previous studies have shown that inverter technology can yield significant energy savings over time (Sukri & Jamali, 2018). Inverters have a significant advantage in maintaining their thermal behavior even after the cooling load decreases, rather than simply due to their ability to reach the target temperature quickly.

According to this study, selecting an air-conditioning system should not be based solely on the equipment's technical specifications but should also consider room characteristics and desired operational objectives. This method provides a more comprehensive basis for selecting the appropriate indoor unit configuration and the most suitable air-conditioning technology. This approach can achieve an ideal balance between thermal comfort, cooling speed, and energy efficiency. These parameters are easily adjustable.

■ CONCLUSION

Airflow distribution and compressor technology are crucial factors in the effectiveness of an air conditioning system. Airflow depends on the unit's position within the room. Efficient air distribution and cooling capacity will affect the occupied area as well as thermal energy consumption. The efficiency of an air-conditioning system should not be based solely on the average room temperature, but rather on the thermal conditions within the area where the system is installed, which can provide a more accurate picture of occupant comfort.

The least efficient configuration is Displacement, which relies on cold air to keep the occupied area below floor level and prevent it from exceeding the target temperature. Additionally, the PM_Above configuration experiences thermal stratification, leading to inaccurate thermostat readings and prolonged compressor operation. In contrast, the PM_Middle configuration achieves optimal overall performance by improving airflow distribution, resulting in more efficient cooling and lower energy consumption for both inverter and non-inverter units. The PM_Middle configuration is considered the optimal choice for installation.

■ REFERENCES

Ali, S. S. S., Kasavan, S., Razman, M. R., Awang, A., & Zarco-Periñán, P. J. (2024). Quantification of household electricity consumption for supporting energy efficiency of urban metabolism: Material flow analysis. *International Journal of Renewable Energy Development*, *13*(5), 960–973. https://doi.org/10.61435/ijred.2024.60267

Almogbel, A., Alkasmoul, F., Aldawsari, Z., Alsulami, J., & Alsuwailem, A. (2020). Comparison of energy consumption between non-inverter and inverter-type air conditioners in Saudi Arabia. *Energy Transitions*, *4*(2), 191–197. https://doi.org/10.1007/s41825-020-00033-y

ASHRAE. (2004). *ANSI/ASHRAE 55:2004 Thermal Environmental Conditions for Human Occupancy*. ASHRAE.

Aziz, H. A. (2017). Comparison between Field Research and Controlled. *Archives of Clinical and Biomedical Research*, *1*(2), 101–104. https://doi.org/DOI:%2010.26502/acbr.50170011

Badan Standarisasi Nasional. (2001). *SNI 03-6572-2001 Tata Cara Perancangan Sistem Ventilasi dan Pengkondisian Udara pada Bangunan Gedung* (SNI SNI 03-6572-2001; 1999.A/BSN-I/HK.50.A/08/2001, p. 60). Badan Standarisasi Nasional.

Barau, A. A. B., Zambri, A. N., Osman, A. A., Ahmed, A. M., Taib, I., & Manshoor, B. (2024). *Observation on Air Flow Distribution in Room by HVAC System using Ansys Fluent CFD Simulation*. *6*(1), 29–37.

Buonocore, C., De Vecchi, R., Scalco, V., & Lamberts, R. (2020). Thermal preference and comfort assessment in air-conditioned and naturally-ventilated university classrooms under hot and humid conditions in Brazil. *Energy and Buildings*, *211*, 109783. https://doi.org/10.1016/j.enbuild.2020.109783

Cahyani, A. D., Nachrowi, N. D., Hartono, D., & Widyawati, D. (2022). Between insufficiency and efficiency: Unraveling households' electricity usage characteristics of urban and rural Indonesia. *Energy for Sustainable Development*, *69*, 103–117. https://doi.org/10.1016/j.esd.2022.06.005

Citadini de Oliveira, C., Catão Martins Vaz, I., & Ghisi, E. (2024). Retrofit strategies to improve energy efficiency in buildings: An integrative review. *Energy and Buildings*, *321*, 114624. https://doi.org/10.1016/j.enbuild.2024.114624

Cosma, A. C., & Simha, R. (2018). Thermal comfort modeling in transient conditions using real-time local body temperature extraction with a thermographic camera. *Building and Environment*, *143*, 36–47. https://doi.org/10.1016/j.buildenv.2018.06.052

De Cian, E., Falchetta, G., Pavanello, F., Romitti, Y., & Sue Wing, I. (2025). The impact of air conditioning on residential electricity consumption across world countries. *Journal of Environmental Economics and Management*, *131*, 103122. https://doi.org/10.1016/j.jeem.2025.103122

Gnecco, V. M., Chiucchiù, A., Mansi, S. A., Pigliautile, I., Cosoli, G., Arnesano, M., & Pisello, A. L. (2025). Exploring acclimation time in test-room environments via physiological indicators: Evolving human-centric personalized comfort measurement procedures. *Building and Environment*, *277*, 112924. https://doi.org/10.1016/j.buildenv.2025.112924

Heidarinejad, G., Fathollahzadeh, M. H., & Pasdarshahri, H. (2015). Effects of return air vent height on energy consumption, thermal comfort conditions and indoor air quality in an under floor air distribution system. *Energy and Buildings*, *97*, 155–161. https://doi.org/10.1016/j.enbuild.2015.04.004

Jin, W., Wang, C., Jiang, Y., Ren, L., Choi, B., & Wang, Z. (2022). Influence of the position of recessed outdoor units and louvre blade angle on the performance of split air conditioners. *Building Services Engineering Research & Technology*, *43*(3), 361–378. https://doi.org/10.1177/01436244211046306

Kar, A. C., & Abedin, M. Z. (2025). Optimization of Indoor Airflow Distribution in Variable Refrigerant Flow Air Conditioning System: A Review. *International Journal of Engineering Materials and Manufacture*, *10*(2), 26–34.

Kementerian ESDM. (2025). *Handbook of Energy & Economic Statistics of Indonesia*. Kementerian ESDM. https://www.esdm.go.id/assets/media/content/content-handbook-of-energy-and-economic-statistics-of-indonesia-2024.pdf

Kementerian Kesehatan. (2016). *Peraturan Menteri Kesehatan Nomor 48 Tahun 2016 tentang Standar Keselamatan dan Kesehatan Kerja Perkantoran* (pp. 1–98) [Peraturan Menteri Kesehatan]. Kementerian Kesehatan. https://peraturan.bpk.go.id/Details/113097/permenkes-no-48-tahun-2016

Khorram, M., Faria, P., Abrishambaf, O., & Vale, Z. (2020). Air conditioner consumption optimization in an office building considering user comfort. *Energy Reports, The 6th International*

Conference on Energy and Environment Research - Energy and Environment: Challenges towards Circular Economy, *6*, 120–126. https://doi.org/10.1016/j.egyr.2019.08.029

Kwag, B. C., Kim, G. T., & Im, D. (2023). Evaluation of the impact of installation environment for a condensing unit of a split-type air conditioner in a plant room of Korean apartment dwellings. *International Journal of Refrigeration*, *156*, 207–218. https://doi.org/10.1016/j.ijrefrig.2023.10.002

Liddle, B., Loi, T. S. A., Owen, A. D., & Tao, J. (2020). Evaluating consumption and cost savings from new air-conditioner purchases: The case of Singapore. *Energy Policy*, *145*, 111722. https://doi.org/10.1016/j.enpol.2020.111722

Maharjan, B., & Rijal, H. B. (2026). Optimal thermal comfort and thermal preferences ranges for office occupants in Japan. *IOP Conference Series: Earth and Environmental Science*, *1582*(1), 012041. https://doi.org/10.1088/1755-1315/1582/1/012041

Pisello, A. L., Pigliautile, I., Andargie, M., Berger, C., Bluyssen, P. M., Carlucci, S., Chinazzo, G., Deme Belafi, Z., Dong, B., Favero, M., Ghahramani, A., Havenith, G., Heydarian, A., Kastner, D., Kong, M., Licina, D., Liu, Y., Luna-Navarro, A., Mahdavi, A., … Wei, S. (2021). Test rooms to study human comfort in buildings: A review of controlled experiments and facilities. *Renewable and Sustainable Energy Reviews*, *149*, 111359. https://doi.org/10.1016/j.rser.2021.111359

PLN. (2025). *Semester I 2025, Konsumsi Listrik Nasional Tumbuh, PLN Catat Penjualan 155,62 TWh*. https://web.pln.co.id/media/siaran-pers/2025/08/semester-i-2025-konsumsi-listrik-nasional-tumbuh-pln-penjualan-15562-twh#:~:text=Sektor Rumah Tangga Jadi Kontributor Utama&text=Jumlah ini tumbuh 5%2C13,ekonomi nasional%2C" pungkas Darmawan.

Sekhar, C., Wargocki, P., Bivolarova, M., & Akimoto, M. (2021, August 10). *Natural vs. Mechanical Ventilation: Comparing CO2 Profiles, Ventilation in Bedrooms* [ASHRAE Journal Newsletter]. ASHRAE. ASHRAE Journal Newsletter,. https://www.ashrae.org/news/ashraejournal/natural-vs-mechanical-ventilation-comparing-co2-profiles-ventilation-in-bedrooms

Setyawati, D., & Setiawan, D. (2024). *Indonesia's expansion of clean power can spur growth and equality*. EMBER. https://ember-energy.org/app/uploads/2024/10/EN-Report-Indonesias-expansion-of-clean-power-can-spur-growth-and-equality.pdf

Sukri, M. F., & Jamali, M. K. (2018). Economic Analysis of An Inverter And Non-Inverter Type Split Unit Air-Conditioners For Household Application. *ARPN Journal Of Engineering And Applied Sciences*, *13*(11), 3749–3757.

Van Craenendonck, S., Lauriks, L., Vuye, C., & Kampen, J. (2018). A review of human thermal comfort experiments in controlled and semi-controlled environments. *Renewable and Sustainable Energy Reviews*, *82*, 3365–3378. https://doi.org/10.1016/j.rser.2017.10.053

Wang, L., Li, G., Gao, J., Fang, X., Wang, C., & Xiong, C. (2023). Case Study: Impacts of Air-Conditioner Air Supply Strategy on Thermal Environment and Energy Consumption in Offices Using BES–CFD Co-Simulation. *Sensors*, *23*(13), 5958. https://doi.org/10.3390/s23135958

Welch, S., Obonyo, E., & Memari, A. M. (2023). A review of the previous and current challenges of passive house retrofits. *Building and Environment*, *245*, 110938. https://doi.org/10.1016/j.buildenv.2023.110938

Yudiartono, Y., Windarta, J., & Adiarso, A. (2023). Sustainable Long-Term Energy Supply and Demand: The Gradual Transition to a New and Renewable Energy System in Indonesia by 2050. *International Journal of Renewable Energy Development*, *12*(2), 419–429. https://doi.org/10.14710/ijred.2023.50361

Zhai, Y., Zhao, S., Yang, L., Wei, N., Xu, Q., Zhang, H., & Arens, E. (2019). Transient human thermophysiological and comfort responses indoors after simulated summer commutes. *Building and Environment*, *157*, 257–267. https://doi.org/10.1016/j.buildenv.2019.04.023